AFRL-AFOSR-VA-TR-2019-0339

Directing Electron Flow and Intermediate Species to Catalytically Active Sites in Engineered Metal/Semiconductor Nanostructures

Stephen Cronin
UNIVERSITY OF SOUTHERN CALIFORNIA

11/01/2019
Final Report

Air Force Research Laboratory
AF Office Of Scientific Research (AFOSR)/ RTB2
Arlington, Virginia 22203
Air Force Materiel Command

REPORT DOCUMENTATION PAGE

Form Approved
OMB No. 0704-0188

1. REPORT DATE *(DD-MM-YYYY)*	2. REPORT TYPE	3. DATES COVERED *(From - To)*
13-11-2019	Final Performance	01 Jun 2015 to 31 May 2019

4. TITLE AND SUBTITLE
Directing Electron Flow and Intermediate Species to Catalytically Active Sites in Engineered Metal/Semiconductor Nanostructures

5a. CONTRACT NUMBER

5b. GRANT NUMBER
FA9550-15-1-0184

5c. PROGRAM ELEMENT NUMBER
61102F

6. AUTHOR(S)
Stephen Cronin

5d. PROJECT NUMBER

5e. TASK NUMBER

5f. WORK UNIT NUMBER

7. PERFORMING ORGANIZATION NAME(S) AND ADDRESS(ES)
UNIVERSITY OF SOUTHERN CALIFORNIA
3720 S FLOWER STREET, THIRD FLOOR
LOS ANGELES, CA 90007 US

8. PERFORMING ORGANIZATION REPORT NUMBER

9. SPONSORING/MONITORING AGENCY NAME(S) AND ADDRESS(ES)
AF Office of Scientific Research
875 N. Randolph St. Room 3112
Arlington, VA 22203

10. SPONSOR/MONITOR'S ACRONYM(S)
AFRL/AFOSR RTB2

11. SPONSOR/MONITOR'S REPORT NUMBER(S)
AFRL-AFOSR-VA-TR-2019-0339

12. DISTRIBUTION/AVAILABILITY STATEMENT
A DISTRIBUTION UNLIMITED: PB Public Release

13. SUPPLEMENTARY NOTES

14. ABSTRACT
We investigate carefully engineered metal/semiconductor nanostructures based on TiO2-passivated III-V compound semiconductors (i.e., GaP, InP, GaAs) to control the flow of electrons and intermediate species to catalytically active sites. The TiO2 passivation layer prevents photocorrosion of the III-V compound surface, providing a viable, long-term stable photocatalyst. Our primary reactions of interest include water splitting and the photocatalytic reduction of CO2 with H2O to various hydrocarbons, which is a complex reaction system requiring up to 8 electrons and many intermediate species, some of which have extremely high energy barriers. This system provides an interesting testbed for studying the control of energy transfer in catalytic processes.
These carefully engineered structures provide control over the electron (hole) energy landscape, directing the flow of electrons to catalytically active sites through built-in fields, arising from a pn-junction formed between the III-V compound semiconductor and TiO2 passivation layer. These structures also enable us to control the adsorption/desorption kinetics of reactant, intermediates, and products to ensure that a high density of intermediates are present at the catalytically active sites. We use vibrational sum frequency generation (vSFG) spectroscopy to identify reaction intermediate species and catalytically active sites on these photocatalytic surfaces. In order to explore and separate various mechanisms of catalysis and enhancement, we will perform a systematic study of sample morphology by varying the surface coverage, size, and shape of metal co-catalyst nanoparticles, and controllably introducing defects to determine their effect on the reaction surface-bound intermediates.

15. SUBJECT TERMS
catalysis, plasmonics

Standard Form 298 (Rev. 8/98)
Prescribed by ANSI Std. Z39.18

16. SECURITY CLASSIFICATION OF:			17. LIMITATION OF ABSTRACT	18. NUMBER OF PAGES	19a. NAME OF RESPONSIBLE PERSON
a. REPORT	b. ABSTRACT	c. THIS PAGE			BERMAN, MICHAEL
Unclassified	Unclassified	Unclassified	UU		19b. TELEPHONE NUMBER *(Include area code)* 703-696-7781

Standard Form 298 (Rev. 8/98)
Prescribed by ANSI Std. Z39.18

AFOSR Final Report 2019

Directing Electron Flow and Intermediate Species to Catalytically Active Sites
June 1, 2015 - May 31, 2019
Profs. Alex Benderskii and Steve Cronin (USC)

Voltage-dependent Water Structure at the Graphene/Water Interface Measured by *in situ* Sum Frequency Generation Spectroscopy

Aqueous interfaces play a crucial role in areas ranging from life sciences, environmental chemistry, and oceanography, to heterogeneous catalysis, electrochemistry, and energy conversion applications. In particular, the solvation properties of interfacial water dictate the chemical equilibria and reaction rates. Our basic understanding of water as a dielectric medium (polar solvent) relies on the assumption of linear response, i.e. that an external perturbation (e.g., electric field) induces a linearly proportional response in the medium (in this example, polarization). Explicit in the linear response assumption is its antisymmetry with respect to the sign of the external field: the response must be of the same magnitude and opposite sign for positive vs. negative applied fields of a given strength. Here, we present surface-selective vibrational sum frequency generation (VSFG) spectroscopy of water (D_2O) near a graphene electrode. Monolayer graphene is transparent and conductive, allowing us to study the response of water to an external electric field under controlled electrochemical conditions. The graphene Raman G-band frequency is used as an internal gauge of the surface charge density. VSFG spectra in the OD-stretch region show a pronounced asymmetry for positive vs. negative electrode charge. At negative charge (below -5×10^{12} e^-/cm^2), a 2700 cm^{-1} peak corresponding to the "free" (non-hydrogen-bonded) OD groups pointing towards graphene surface is observed. At neutral or positive electrode potentials, the "free OD" peak is absent, and the spectra are dominated by the broad peaks of the hydrogen-bonded OD-stretch (2300-2650 cm^{-1}). Evolution of VSFG spectra as a function of the external electric field is connected to the linear susceptibility (and the dielectric constant) by the Miller's rule.[1] The observed deviation from the linear response to electric fields of the order of $\pm3\times10^8$ V/m therefore calls into question the validity of considering interfacial water as a simple dielectric medium.

Liquid water owes most of its physical and chemical properties to the dynamical network of aqueous hydrogen bonds. The latter represents a subtle interplay between local interactions reflecting the geometry of the water molecules (the charge distribution and polarizability of the OH-bonds and lone pairs), and the long-range electrostatic (dipole-dipole) interactions. This interplay underlies the complexity of water's response to an electric field. The molecular-level picture of this response is paramount to our understanding of its properties as a dielectric medium[2] (in the case of an externally applied E-field) and as a polar solvent (in the case of the E-field around a solute molecule).[3] Application of an external electric field of a planar electrode is therefore a useful tool for studying the H-bond network of water, by quantifying the magnitude of the response relative to the strength of the perturbation. A simplistic picture is partial alignment of the water dipoles by the electric field, a result of competition between the torque produced on a given molecule by the field-dipole interaction and the hydrogen bonds between this molecule and its neighbors, which, in the absence of the field, yield the isotropic orientational distribution in bulk water.

Vibrational spectroscopy of water is a natural match for studying aqueous hydrogen bonds, mostly due to the well-researched relationship between the frequency shifts of the OH/OD-stretch modes and the local hydrogen-bonding environment.[4-6] Surface-selective vibrational sum

frequency generation spectroscopy (VSFG) has been applied to study the molecular structure of water at charged interfaces such as mineral surfaces (where the surface charge can be adjusted by varying the pH of the solution)[7-9] or monolayers of surfactants with charged head groups.[10-12]

The fundamental asymmetry of the interfacial environment makes aqueous H-bonds at interfaces different from bulk water. We can classify the factors underlying the interfacial asymmetry into three categories: (1) geometric termination of the 3-dimensional network of the H-bonds at the interface - which may be planar or have nanometer or molecular scale morphology (e.g., capillary waves, corrugated/nanostructured surfaces, and/or shape and spatial arrangement of the surfactant headgroups) (2) surface electrostatics – effects of the surface charge and the spatial distributions of counterions (if any) in the water phase, and (3) specific local interactions of interfacial water molecules with the molecules (e.g., hydrophilic vs. hydrophibic) of the other phase.

The electrostatic effects (type 2) due to the field of a planar charged surface – subject of our present study – would be generally applicable to all charged interfaces. It would therefore be useful to disentangle these from other interactions. However, this is difficult for the previously studied systems, where all three factors are simultaneously present, e.g. hydrogen bonding of water to the hydrophilic surfactant head groups or hydroxyl moieties on a mineral surface. The situation is further complicated by the morphology of the surface (especially in the case of surfactant monolayers) and the presence of counterions,[2,5] whose spatial distribution affects the local electric fields.

Our approach is to utilize a monolayer graphene electrode to apply charge to interfacial water and measure the response using *in situ* vibrational sum frequency generation (VSFG) spectroscopy under controlled electrochemical conditions. This system enables us to continuously vary the surface charge from negative to positive without changing the chemical composition of the surface. Monolayer graphene is atomically flat, conductive, chemically inert, and nearly transparent (2.3% absorbance) throughout the visible and infrared spectral ranges.[13] Furthermore, there has been significant recent interest in water-graphene interactions for applications such as water purification and electric power generation.[14, 15]

Our experimental cell is schematically depicted in Figure 1A. The monolayer graphene electrode is supported on a CaF_2 substrate (1 mm thick), which forms the top window of the electrochemical flow-cell, with graphene facing the water (D_2O) under the window. The incoming visible (800 nm) and infrared laser beams access the graphene/water interface through the CaF_2 window, and the VSFG signal generated in the reflection direction exits the cell through the same window. We use the broad-band VSFG technique, which combines a femtosecond mid-infrared pulse centered at the OD-stretch band, 2500 cm^{-1} (FWHM = 375 cm^{-1}) with a narrow-band (picosecond) visible pulse at 800 nm generated by a 4f-stretcher (~2 ps, FWMH = 10 cm^{-1}).[16] D_2O (Cambridge Isotopes Laboratories Inc., 99.9% purity) was continually flowed with a peristaltic pump (Fisher Scientific, Model: 13-876-2) at 6 mL/min to reduce laser-induced heating on the sample. No electrolyte was added in our experiments.

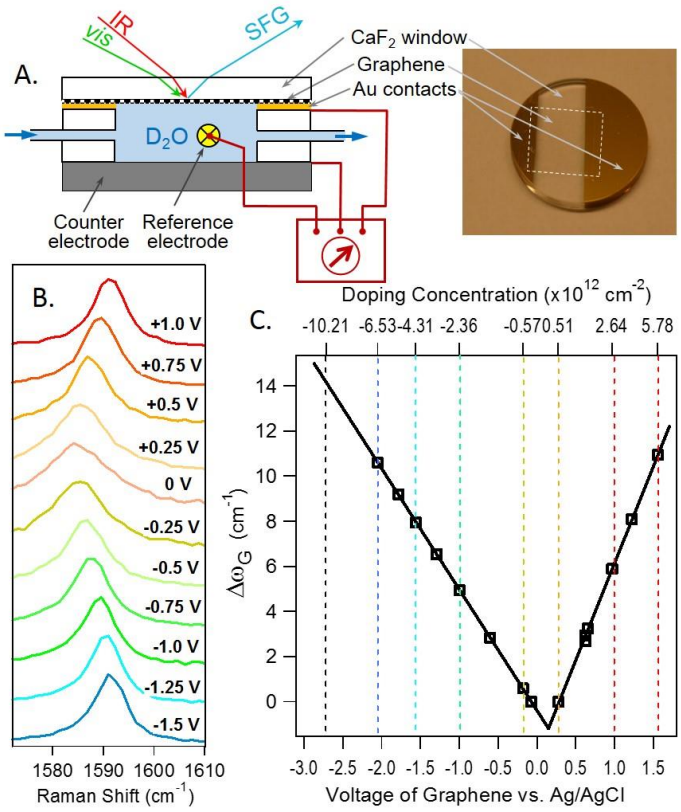

Figure 1. A. Schematic diagram of the experimental electrochemical flow-cell with a monolayer graphene electrode and gold contact strips supported on a CaF_2 top window. The counter electrode is glassy carbon, and the reference electrode is Ag/AgCl. **B.** Raman spectra of the G-band of graphene electrode, recorded as a function of electrochemical potential (vs. Ag/AgCl). The spectra are vertically off-set for clarity. **C.** The G-band central frequency vs. electrode potential. Squares: experimental points; solid lines: linear fit. The vertical grid lines and the top axis relate the voltages that were used in the VSFG experiments to the doping concentrations of the graphene electrode.

Two strips of evaporated gold were deposited on each side of the graphene sheet (1.5 cm × 1 cm) and serve as electrical contacts (Figure 1A). The Teflon spacer that made up the cell is 8 mm thick, and the cell bottom was a glassy carbon counter electrode, which forms a two-terminal electrochemical cell. Additional measurements were performed in a three-terminal configuration, with a Ag/AgCl reference electrode inserted through the side wall of the Teflon cell, between the graphene working electrode and the glassy carbon counter electrode. At the same time, the in-plane resistance of the monolayer graphene (measured between the two gold contacts, typically 1–2 kΩ) was monitored to ensure no degradation of the graphene monolayer occurs during the course of the measurements.

The frequency shift of the G-band Raman mode of monolayer graphene provides an intrinsic measure of the excess charge density via a well-established relationship[17] given below in Eq. (1). *In situ* Raman spectra of the graphene electrode under applied electrochemical potentials were collected using a Renishaw micro-Raman spectrometer using both two-terminal and three-terminal configurations. The G-band frequency of the graphene, around 1585 cm^{-1}, reaches a

minimum at the charge neutral point around +0.1 V vs. Ag/AgCl. The G-band Raman frequency blue-shifts linearly as a function of the applied potential, as plotted in Figure 1B. From the G-band frequency shift $\Delta\omega_G$, Figure 1C, the Fermi energy E_f and doping concentration n were calculated using the following relations:[18]

$$\begin{aligned} &\text{Electrons: } E_f = 21\Delta\omega_G + 75 \ \ [\text{cm}^{-1}] \\ &\text{Holes: } \quad E_f = -18\Delta\omega_G - 83 \ \ [\text{cm}^{-1}] \\ &n = \left(\frac{E_f}{11.65}\right)^2 10^{10} \ \ [\text{cm}^{-2}] \end{aligned} \tag{1}$$

The surface charge density $\sigma=ne$ was confirmed by independent electrode capacitance measurements.[18] Further details of the graphene electrode preparation, VSFG set-up, design and calibration of the electrochemical cell, and the laser setup are presented in the Supporting Information.

Voltage-dependent VSFG spectra of D_2O at the graphene interface (Figure 2) were collected using the SSP polarization combination (SFG, visible, and IR beams, respectively). Applying a negative bias dopes the graphene with electrons, while a positive bias dopes the graphene with holes, yielding negatively- or positively-charged interfaces, respectively (Figure 1C). The most striking feature of the observed spectra is their asymmetry with respect to positive vs. negative applied fields. At –1.6 V (vs. Ag/AgCl) and below, the VSFG spectra of the graphene-D_2O interface exhibits one relatively narrow peak (FWHM ≈ 30 cm^{-1}) at 2697±3 cm^{-1}, corresponding to the free-OD stretch. This narrow feature is a local mode assigned to water in the topmost monolayer, where one OD-group points away from the bulk and does not hydrogen bond (i.e., dangling or free-OD).[19, 20] For voltages of –1.0 V and above, the free-OD feature is absent and only hydrogen-bonded peaks are observed in the 2300 – 2650 cm^{-1} region.[6, 21]

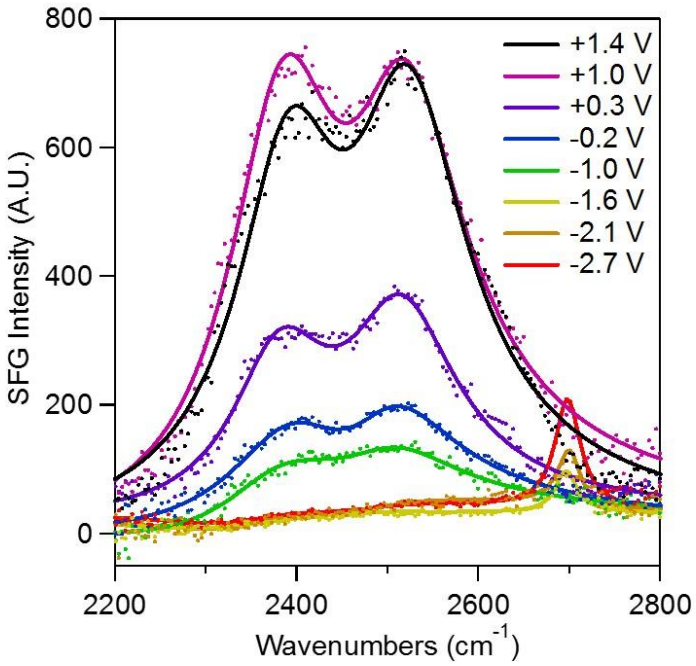

Figure 2. VSFG spectra of the OD-stretch of D_2O at the graphene electrode, at different potentials vs. Ag/AgCl. The spectra were recorded using SSP polarization combination (IR, visible, SFG). Solid lines show the fit to the model with interfering surface and bulk contributions described in text, Eq. (4). The potentials are converted to surface charge densities according to Figure 1C.

Our spectra near the charge-neutral point are consistent with the experimental work of Dhinojwala *et al.*,[22] who measured VSFG spectra of H_2O in contact with graphene surface in an open circuit configuration. In both their and our measurements, the free-OH/OD peaks were absent. This is, however, in contradiction with theoretical studies of the hydrophobic graphene-water interface, which predict the free OD feature at the neutral potential.[23]

Although some of the applied voltages are outside of the range of electrochemical stability of water, graphene is an inert electrode and the rate of the water splitting is slow, as indicated by the relatively small current flowing through the cell – below 100 μA at −2.7 V for the graphene electrode area of 1.5 cm^2.[1] An equilibration time of 2 min was allowed to elapse at each voltage to ensure the measurements are performed in the steady-state. The applied voltages were randomly staggered (instead of stepping the voltage in a single direction) to rule out any effects associated with irreversible changes to the electrode, and the 0.3 V spectrum was periodically retaken to ensure that there was no drift in the signal over time. We find no evidence of water trapped between the graphene and CaF_2 substrate: experiments performed on an empty ("dry") cell yielded no VSFG signal. Also, the signal vanished completely by isotopically diluting D_2O with H_2O, as described in the SI.

While VSFG ($\omega_{SFG} = \omega_1 + \omega_2$) is normally a second-order nonlinear optical process, the static electric field (E_0, $\omega_3 = 0$) at a charged interface results in a third-order contribution to the signal:

$$E_{SFG} = \chi^{(2)} : E_{\omega_1} E_{\omega_2} + \chi^{(3)} : E_{\omega_1} E_{\omega_2} E_0 \qquad (2)$$

It is generally agreed that the $\chi^{(2)}$ contribution originates from a few top-most monolayers of water[12, 20, 24, 25] (beyond that, isotropic orientational distribution of bulk water is restored, resulting in zero SFG signal). On the contrary, the region contributing the $\chi^{(3)}$ signal may extend into the liquid as far at the static field $E_0(z)$, which decays over the Debye screening length.[10, 25, 26] Following Shen and Tian,[12] we spatially separate the $\chi^{(3)}$ contribution into the 'surface' part originating from the same interfacial region as $\chi^{(2)}$, and a 'bulk' part, Figure 3A. The surface contribution $\chi_s^{(3)}$ can be thought of as the change in the interfacial second-order susceptibility due to the static field

$$\chi_s^{(2)}(E_0) = \chi_s^{(2)}(0) + \chi_s^{(3)} E_0 \qquad (3)$$

Most of the molecular dynamics simulations of the graphene/water interface show a vacuum gap of ~3 Å between the top-most layer of water and the graphene plane.[23, 27] Accordingly, the electric field experienced by the top monolayer of water is estimated as $E_0(0) = \frac{\sigma}{2\varepsilon_0 \varepsilon}$ (with ε=1) where σ is the surface charge density obtained from the Raman G-band shift measurements (Figure 1C).

The bulk contribution $\chi_b^{(3)}$ is integrated over the depth *z*, which results in the celebrated Eisenthal relationship on the surface potential $\Phi_0(0)$.[28] When the Debye screening length is comparable to the light wavelength, phase retardation effects become important in the interference of the bulk $\chi_b^{(3)}$ contribution and the surface signal,[12] for which a formal expression was recently derived:[25, 26]

[1] At this current level, one electron is transferred per area occupied by a single water molecule (~10 $Å^2$) every 5 seconds, on average. The time scale of the spectroscopic measurement is ~1 ps.

$$I_{SFG} \propto \left| \chi_s^{(2)} + \frac{\kappa e^{i\varphi}}{\sqrt{\kappa^2 + (\Delta k_z)^2}} \chi_b^{(3)} \Phi_0(0) \right|^2, \quad \varphi = \arctan\left(\frac{\Delta k_z}{\kappa} \right) \tag{4}$$

where κ is the inverse of the Debye screening length and $\Delta k_z = k_{SFG,z} - k_{1,z} - k_{2,z}$ is the inverse of the coherence length of the SFG process. In our case of pure D_2O (no electrolyte added), the Debye length is of the order of 1 μm.

Recent studies of several charged aqueous interfaces (various lipid monolayers and mineral surfaces) have concluded that the bulk $\chi_b^{(3)}$ contribution has nearly the same spectral line shape regardless of the chemical nature of the surface, and follows the linear response, i.e. is proportional to the static field (and the potential) of the surface.[12, 24, 25] We used this spectral shape of the bulk $\chi_b^{(3)}$ contribution,[12, 21, 25] in fitting our VSFG spectra to Eq. (4), allowing us to extract the spectra of the interfacial water as a function of the surface field, $\chi_s^{(2)}(E_0)$.

The results of the spectral decomposition are presented in Figure 3B,C, where the imaginary parts of the bulk and surface contributions are shown. Consistent with the previous studies in both shape and sign, the bulk contribution $\mathrm{Im}\left[\chi_b^{(3)}\right]$, represented by two broad Lorentzians at 2365 cm^{-1} and 2510 cm^{-1} (FWHM= 150 cm^{-1}), resembles the linear absorption spectrum of bulk water and scales linearly with the applied potential $\Phi_0(0)$.

The extracted surface contribution $\chi_s^{(2)}(E_0)$ does not follow the linear response behavior, showing a pronounced asymmetry with respect to positive vs. negative surface charge. We have fitted the $\chi_s^{(2)}(E_0)$ spectra using 3 Lorentzians: one narrow peak at 2697 cm^{-1} representing the "free-OD" species, and two broader red-shifted peaks at ~2350 cm^{-1} and ~2500 cm^{-1} representing H-bonded structures. Figure 3 D-F shows the amplitudes of these spectral components as a

function of the applied potential. This implies that the surface signal does not behave according to Eq. (3).

We note that although our VSFG measurements were performed at the intensity level, the signs of the extracted spectral components are consistent with all previous studies that used optical heterodyne detection.[8, 11, 12, 20] If we define the sign of $\mathrm{Im}\left[\chi^{(2)}\right]$ of the free OD feature as positive (free OD groups always point up), then the bulk contribution $\mathrm{Im}\left[\chi_b^{(3)}\right]$ is positive at negatively charged surfaces and negative at positively charged surfaces. At the positive potentials, the sign of the hydrogen-bonded part of the surface contribution also goes negative.

The well-established Miller's rule in nonlinear optics[1] is a proportionality relationship between a nonlinear susceptibility and a product of the first-order (linear) susceptibilities at constituent frequencies. It works well for off-resonant response and therefore for DC fields, as was already pointed out in Miller's original paper.[1] A straightforward extension of the Miller's rule to our case suggests that the change of the second-order susceptibility in response to the static field of a charged surface, Eq. (3), is proportional to the linear DC susceptibility of the interfacial layer,

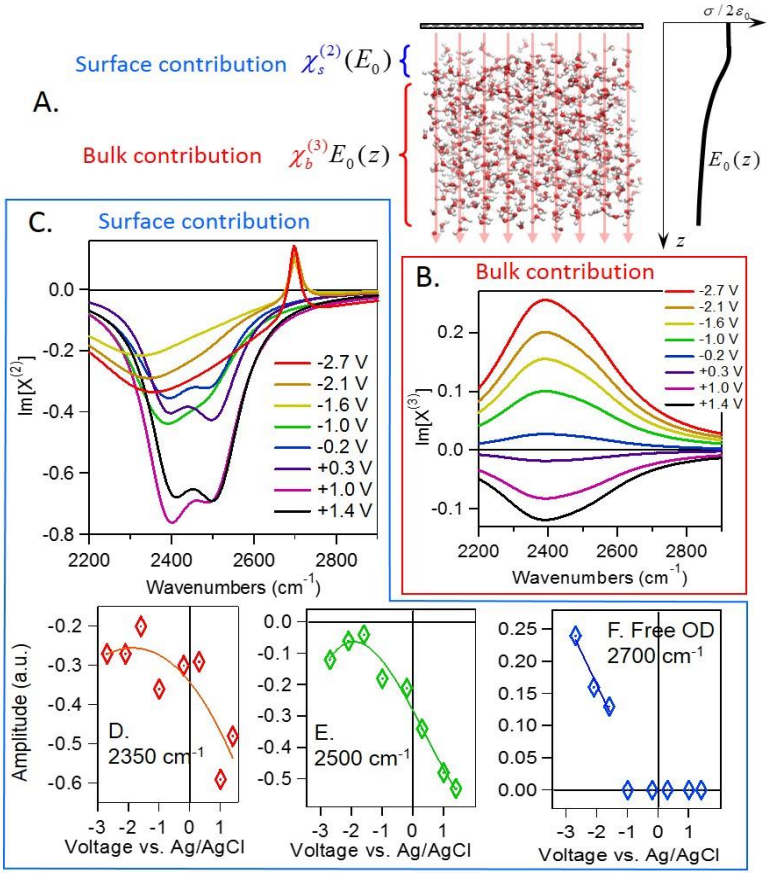

Figure 3. A. Schematic illustration of the spatial separation of the surface and bulk contributions to the VSFG signal at the water/graphene electrode interface, and the depth-dependence of the electric field $E_0(z)$. **B.** As shown by previous studies, the bulk contribution resembles bulk water absorption spectrum and behaves as expected according to the linear response approximation: charge reversal results in the sign reversal of the response. **C.** The extracted surface contribution $\chi_s^{(2)}(E_0)$ as a function of electrode potential (plotted here is its imaginary part) shows pronounced deviations from the linear response behavior. Bottom panel (**D, E, F**): Spectral amplitudes of the three Lorentzian peaks used to fit the surface contribution (C.), as a function on electrode potential. **D, E.** The amplitudes of the peaks centered at 2350 cm^{-1} and 2500 cm^{-1}, respectively. Solid lines show a 4th order polynomial fit. **F.** The amplitude of the free-OD peak centered at 2694 cm^{-1}; as evident from the raw spectra (Figure 2), this peak is absent at potentials ≥ –1.0V vs. Ag/AgCl.

$$\chi_s^{(3)}(\omega_1,\omega_2,0) \propto \chi_s^{(2)}(\omega_1,\omega_2)\chi_s^{(1)}(0) \qquad (5)$$

(Note that we only consider the off-resonant zero-frequency component for the proportionality relationship).[2] The linear susceptibility is connected to the dielectric constant of the interfacial layer, $\varepsilon_s = 1 + 4\pi\chi_s^{(1)}(0)$. Our observation that the VSFG spectra of the interfacial water do not obey the linear response behavior (3), thus, suggests that the linear dielectric response may be inadequate in describing how this layer responds to external field.

The deviation of the electrostatics of interfacial water from the linear response behavior would have multiple consequences in both theoretical and computer simulation studies, and practical applications. At the surface charge densities explored in our study (from -10^{13} e^-/cm^2 to $+5\times10^{12}$ e^-/cm^2, i.e. –0.016 to +0.008 C/m^2), the electric field strengths are of the order of ±0.03 V/Å at the interface and decay into the bulk. Dielectric saturation is predicted to occur in bulk water for E-fields on the order of 10^9 V/m (0.1 V/Å),[29] and is expected to manifest itself as a simple monotonic decrease of the effective dielectric constant.[3] The bulk contribution $\chi_b^{(3)}$ obeys the linear behavior, consistent with this limit, since the deeper water layers experience the static field weaker than at the interface, well below the dielectric saturation limit. The interfacial water, however, seems to deviate from the linear behavior in much weaker fields, and in a non-monotonic fashion. We also note that the surface charge density in many commonly occurring systems, such as phospholipid monolayers and bilayers, can be of the order of one elementary charge per <100 $Å^2$, while here it is less than one elementary charge per 1000 $Å^2$.

The order of magnitude of the dielectric saturation field in liquid water, ~10^9 V/m, can be qualitatively understood as being comparable to the field imposed by the nearest neighbor molecules. From this standpoint, it makes sense that the interfacial water should tend to exhibit non-linear effects at weaker fields, doe to the smaller average number of nearest neighbors.

It is interesting to consider possible molecular mechanisms responsible for the non-linear behavior of interfacial water. One obvious mechanistic insight is offered by the disappearance of the free OD feature at neutral or positive potentials. At a negatively charged interface, the free OD moiety likely points towards the graphene, into the vacuum gap, thus appearing as a narrow blue-shifted peak in the VSFG spectra. As the surface becomes neutral or positive, the free OD species orient away from graphene and towards bulk water, where they are more likely to find H-bonding partners and no longer contribute to the free-OD peak. This asymmetry is one of the mechanisms of the linear response breakdown. Field-induced interconversion between different hydrogen-bonding classes can be viewed as a phase transition of interfacial water, which was first suggested based on temperature-jump relaxation measurements in 1980's.[30] We hope that our work will stimulate further theoretical and experimental studies of the molecular mechanisms underpinning the unusual behavior of interfacial water.

CO Adsorption on Roughened Gold Surfaces

During the reporting period, we have investigated CO adsorption on roughened gold surfaces under ambient conditions using vibrational sum frequency generation (vSFG) spectroscopy of the CO stretch mode, whose frequency is sensitive to the nature of the adsorption site. It is well known that CO does not adsorb on atomically flat gold and other metals at room

[2] The proportionality does not imply that the second-order susceptibility $\chi_s^{(2)}(\omega_1, \omega_2)$ is related to the residual spectrum at zero field, $\chi_s^{(2)}(0)$ in Eq. (3).

[3] Defined as a derivative of the induced polarization vs. applied static electric field.

temperature. However, we discovered that on roughened gold, CO adsorption occurs at metastable sites that are annealed away at temperature as low as 120°C. Two sites were observed and assigned with the help of the Density Functional Theory (DFT) calculations: the stronger peak at 1960 cm^{-1} corresponding to the bridge site at the step-edge, and 2020 cm^{-1} corresponding to atop site at step-edge. As shown in Figure 4, CO adsorption is significantly enhanced in the presence of water vapor, indicating cooperativity in CO + H_2O adsorption at these defect sites. DFT calculations suggest a mechanism for this cooperativity by polar water molecule promoting charge transfer between nearby adsorbed CO and the metal surface.

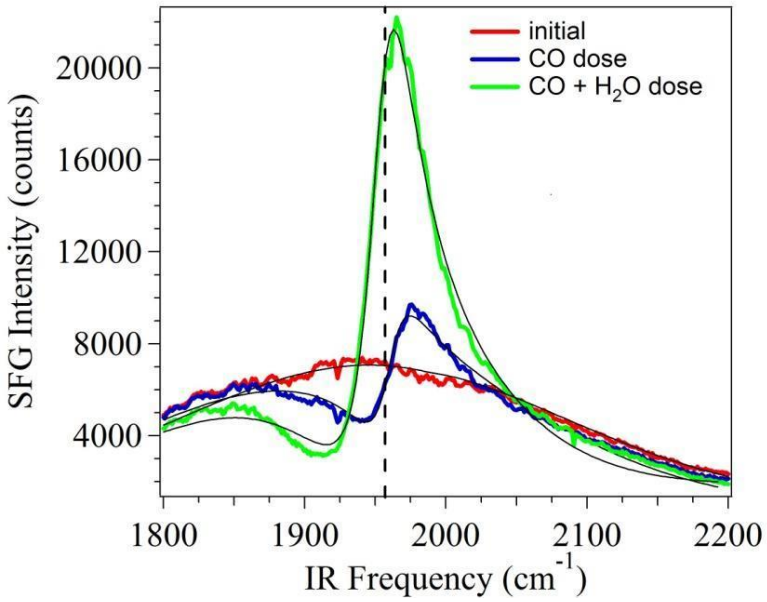

Figure 4. VSFG spectra of piranha-cleaned continuous vapor-deposited gold (sample 1). Spectra measured before dosing adsorbates (red line), after dosing CO only (blue), and after co-dosing CO and H_2O (green) are plotted in the Figure. The black lines are spectral fits.

The experimental results suggest the possible role of metastable sites or defects in CO binding. Figure 5 shows the effect of repeated thermal annealing cycles on subsequent CO + H_2O adsorption. In the leftmost panel, the CO peak at 1950 cm^{-1} was annealed away by heating to 120 °C, as the black spectrum (after flash annealing) shows almost no CO peak remaining. Upon a second dosing with CO + H_2O, the CO peak reappears (blue spectrum, center panel), albeit with a weaker amplitude (decreased by a factor of 2). A second thermal annealing at 120 °C once again completely desorbs CO from the Au surface (orange spectrum). Upon the third and final dosing with CO + H_2O, the CO peak regenerates (purple spectrum, right panel), although with a much weaker amplitude than before (decreased by a factor of 8). Subsequent annealing removes the adsorption sites for CO.

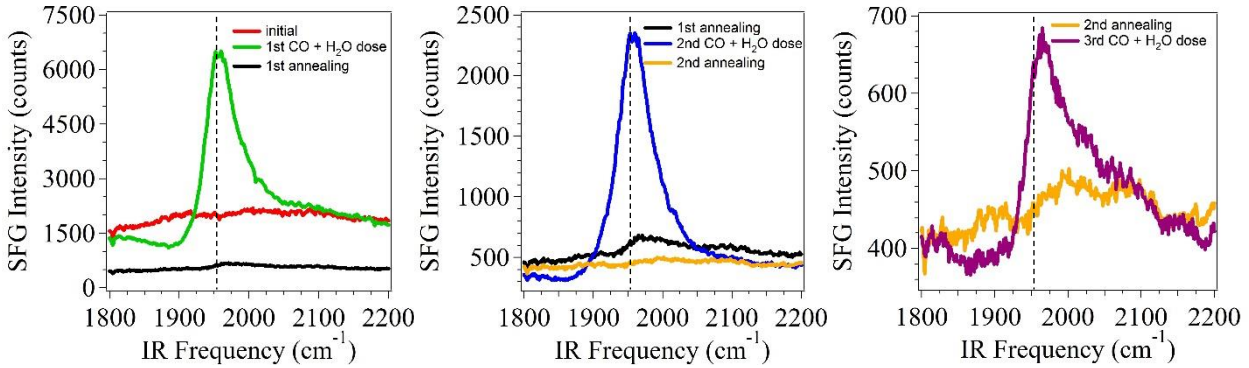

Figure 5. VSFG spectra of piranha-cleaned rough Au surface acquired before dosing adsorbates (red spectrum), after first co-dosing of CO and H_2O vapor (green), after first flash annealing (black), after second co-dosing of CO and H_2O vapor (blue), after second flash annealing (orange), and after third co-dosing of CO and H_2O vapor (purple).

Sensing Local pH and Ion Concentration at Graphene Electrode Surfaces using *in situ* Raman Spectroscopy

In addition to SFG spectroscopy, we also report a novel approach to probe the local ion concentration at graphene/water interfaces using *in situ* Raman spectroscopy.[31] Here, the upshifts observed in the G band Raman mode under applied electrochemical potentials are used to determine the charge density in the graphene sheet. For voltages up to ±0.8 V vs. NHE, we observe substantial upshifts in the G band Raman mode by as much as 19 cm^{-1}, which corresponds to electron and hole carrier densities of 1.4×10^{13} cm^{-2} and Fermi energy shifts of ±430 meV. The charge density in the graphene electrode is also measured independently using the capacitance-voltage characteristics (i.e., Q = CV), and is found to be consistent with those measured by Raman spectroscopy. From charge neutrality requirements, the ion concentration in solution per unit area must be equal and opposite to the charge density in the graphene electrode. Based on these charge densities, we estimate the local ion concentration as a function of electrochemical potential in both pure DI water and 1 M KCl solutions, which span a pH range from 3.8 to 10.4 for pure DI water and net ion concentrations of ±0.7 mol L^{-1} for KCl under these applied voltages.

Prevention of Surface Recombination by Electrochemical Tuning of TiO_2-passivated Photocatalysts

We reported a systematic study of photoluminescence (PL) spectroscopy of TiO_2-passivated GaAs as a function of electrochemical potential in an ionic liquid solution.[32] We observe a 7X increase in the PL intensity as the GaAs transitions from accumulation to depletion due to the applied potential. We attribute this to the excellent control over the surface Fermi level enabled by the high capacitance of the electrochemical double layer and TiO_2. This allows us to control the surface carrier concentration and corresponding non-radiative recombination rate. In addition to photoluminescence (PL) spectroscopy, we also measured the capacitance-potential (i.e., C-V) characteristics of these samples, which indicate flat band potentials that are consistent with these regimes of ion accumulation observed in the photoluminescence measurements. We have also performed electrostatic simulations of these C-V characteristics, which provide a detailed and quantitative picture of the conduction and valence band profiles and charge

distribution at the surface of the semiconductor. These simulations also enable us to determine the range of potentials over which the semiconductor surface experiences depletion, inversion, and accumulation of free carriers. Based on these simulations, we can calculate the Shockley-Read-Hall recombination rate and model the PL intensity as a function of voltage. This approach allows us to explain our experimental data well.

Hot Electron-driven Photocatalytic Water Splitting

We also reported measurements of photocatalytic water splitting using Au films with and without TiO_2 coatings.[33] In these structures, a thin (3–10 nm) film of TiO_2 is deposited using atomic layer deposition (ALD) on top of a 100 nm thick Au film. We utilize an AC lock-in technique, which enables us to detect the relatively small photocurrents (~μA) produced by the short-lived hot electrons that are photoexcited in the metal. Under illumination, the bare Au film produces a small AC photocurrent (<1μA) for both the hydrogen evolution reaction (HER) and the oxygen evolution reaction (OER) due to hot electrons and hot holes, respectively, that are photoexcited in the Au film. The samples with TiO_2 produce a larger AC photocurrent indicating that hot electrons are being injected from the metal into the TiO_2 semiconductor where they then reduce hydrogen ions in solution forming H_2 (i.e., $2H^+ + 2e^- \rightarrow H_2$). The AC photocurrent exhibits a narrow peak when plotted as a function of reference potential, which is a signature of hot electrons. Here, we photoexcite a monoenergetic source of hot electrons, which produces a peak in the photocurrent, as the electrode potential is swept through the resonance with the redox potential of the desired half-reaction. This stands in contrast to conventional bulk semiconductor photocatalysts, whose AC photocurrent saturates beyond a certain potential (i.e., light limited photocurrent). The photocurrents produced at the metal–liquid interface are smaller than those of the metal–semiconductor system, mainly because, in the metal–semiconductor system, there is a continuum of energy and momentum states that each hot electron can be injected into, while for an ion in solution, the number of energy and momentum states are very small

References

1. Miller, R.C., *Optical 2nd Harmonic Generation in Piezoelectric Crystals.* Applied Physics Letters, **5**, 17-19 (1964).
2. Wyman, J., *Measurements of the dielectric constants of conducting media.* Physical Review, **35**, 623-634 (1930).
3. Kirkwood, J.G., *The dielectric polarization of polar liquids.* Journal of Chemical Physics, **7**, 911-919 (1939).
4. Fecko, C.J., J.D. Eaves, J.J. Loparo, A. Tokmakoff and P.L. Geissler, *Ultrafast hydrogen-bond dynamics in the infrared spectroscopy of water.* Science, **301**, 1698-1702 (2003).
5. Bakker, H.J. and J.L. Skinner, *Vibrational Spectroscopy as a Probe of Structure and Dynamics in Liquid Water.* Chemical Reviews, **110**, 1498-1517 (2010).
6. Nihonyanagi, S., T. Ishiyama, T. Lee, S. Yamaguchi, M. Bonn, A. Morita and T. Tahara, *Unified Molecular View of the Air/Water Interface Based on Experimental and Theoretical chi((2)) Spectra of an Isotopically Diluted Water Surface.* Journal of the American Chemical Society, **133**, 16875-16880 (2011).
7. Du, Q., E. Freysz and Y.R. Shen, *Vibrational-Spectra of Water-Molecules at Quartz Water Interfaces.* Physical Review Letters, **72**, 238-241 (1994).

8. Myalitsin, A., S.H. Urashirna, S. Nihonyanagi, S. Yamaguchi and T. Tahara, *Water Structure at the Buried Silica/Aqueous Interface Studied by Heterodyne-Detected Vibrational Sum-Frequency Generation.* Journal of Physical Chemistry C, **120**, 9357-9363 (2016).
9. Schaefer, J., G. Gonella, M. Bonn and E.H.G. Backus, *Surface-specific vibrational spectroscopy of the water/silica interface: screening and interference.* Physical Chemistry Chemical Physics, **19**, 16875-16880 (2017).
10. Gragson, D.E. and G.L. Richmond, *Investigations of the structure and hydrogen bonding of water molecules at liquid surfaces by vibrational sum frequency spectroscopy.* Journal of Physical Chemistry B, **102**, 3847-3861 (1998).
11. Nihonyanagi, S., S. Yamaguchi and T. Tahara, *Direct evidence for orientational flip-flop of water molecules at charged interfaces: A heterodyne-detected vibrational sum frequency generation study.* Journal of Chemical Physics, **130**, 204704 (2009).
12. Wen, Y.C., S. Zha, X. Liu, S.S. Yang, P. Guo, G.S. Shi, H.P. Fang, Y.R. Shen and C.S. Tian, *Unveiling Microscopic Structures of Charged Water Interfaces by Surface-Specific Vibrational Spectroscopy.* Physical Review Letters, **116**, 016101 (2016).
13. Nair, R.R., P. Blake, A.N. Grigorenko, K.S. Novoselov, T.J. Booth, T. Stauber, N.M.R. Peres and A.K. Geim, *Fine structure constant defines visual transparency of graphene.* Science, **320**, 1308-1308 (2008).
14. Seo, D.H., S. Pineda, Y.C. Woo, M. Xie, A.T. Murdock, E.Y.M. Ang, Y. Jiao, M.J. Park, S.I. Lim, M. Lawn, F.F. Borghi, Z.J. Han, S. Gray, G. Millar, A.J. Du, H.K. Shon, T.Y. Ng, and K. Ostrikov, *Anti-fouling graphene-based membranes for effective water desalination.* Nature Communications, **9**, 683 (2018).
15. Dhiman, P., F. Yavari, X. Mi, H. Gullapalli, Y.F. Shi, P.M. Ajayan and N. Koratkar, *Harvesting Energy from Water Flow over Graphene.* Nano Letters, **11**, 3123-3127 (2011).
16. Stiopkin, I.V., H.D. Jayathilake, C. Weeraman and A.V. Benderskii, *Temporal effects on spectroscopic line shapes, resolution, and sensitivity of the broad-band sum frequency generation.* Journal of Chemical Physics, **132**, 234503 (2010).
17. Froehlicher, G. and S. Berciaud, *Raman spectroscopy of electrochemically gated graphene transistors: Geometrical capacitance, electron-phonon, electron-electron, and electron-defect scattering.* Physical Review B, **91**, 205413 (2015).
18. Shi, H.T., N. Poudel, B.Y. Hou, L. Shen, J.H. Chen, A.V. Benderskii and S.B. Cronin, *Sensing local pH and ion concentration at graphene electrode surfaces using in situ Raman spectroscopy.* Nanoscale, **10**, 2398-2403 (2018).
19. Du, Q., R. Superfine, E. Freysz and Y.R. Shen, *Vibrational Spectroscopy of Water at the Vapor Water Interface.* Physical Review Letters, **70**, 2313-2316 (1993).
20. Stiopkin, I.V., C. Weeraman, P.A. Pieniazek, F.Y. Shalhout, J.L. Skinner and A.V. Benderskii, *Hydrogen bonding at the water surface revealed by isotopic dilution spectroscopy.* Nature, **474**, 192-195 (2011).
21. Ohno, P.E., H.F. Wang, F. Paesani, J.L. Skinner and F.M. Geiger, *Second-Order Vibrational Lineshapes from the Air/Water Interface.* Journal of Physical Chemistry A, **122**, 4457-4464 (2018).
22. Singla, S., E. Anim-Danso, A.E. Islam, Y. Ngo, S.S. Kim, R.R. Naik and A. Dhinojwala, *Insight on Structure of Water and Ice Next to Graphene Using Surface-Sensitive Spectroscopy.* Acs Nano, **11**, 4899-4906 (2017).

23. Ohto, T., H. Tada and Y. Nagata, *Structure and dynamics of water at water-graphene and water-hexagonal boron-nitride sheet interfaces revealed by ab initio sum-frequency generation spectroscopy.* Physical Chemistry Chemical Physics, **20**, 12979-12985 (2018).
24. Joutsuka, T., T. Hirano, M. Sprik and A. Morita, *Effects of third-order susceptibility in sum frequency generation spectra: a molecular dynamics study in liquid water.* Physical Chemistry Chemical Physics, **20**, 3040-3053 (2018).
25. Ohno, P.E., H.F. Wang and F.M. Geiger, *Second-order spectral lineshapes from charged interfaces.* Nature Communications, **8**, 1032 (2017).
26. Gonella, G., C. Lutgebaucks, A.G.F. de Beer and S. Roke, *Second Harmonic and Sum-Frequency Generation from Aqueous Interfaces Is Modulated by Interference.* Journal of Physical Chemistry C, **120**, 9165-9173 (2016).
27. Ostrowski, J.H.J. and J.D. Eaves, *The Tunable Hydrophobic Effect on Electrically Doped Graphene.* Journal of Physical Chemistry B, **118**, 530-536 (2014).
28. Ong, S.W., X.L. Zhao and K.B. Eisenthal, *Polarization of Water-Molecules at a Charged Interface - 2nd Harmonic Studies of the Silica Water Interface.* Chemical Physics Letters, **191**, 327-335 (1992).
29. Alper, H.E. and R.M. Levy, *Field-Strength Dependence of Dielectric Saturation in Liquid Water.* Journal of Physical Chemistry, **94**, 8401-8403 (1990).
30. Benderskii, V.A. and G.I. Velichko, *Temperature jump in electric double-layer study .1. Method of measurements.* Journal of Electroanalytical Chemistry, **140**, 1-22 (1982).
31. Shi, H., N. Poudel, B. Hou, L. Shen, J. Chen, A. Benderskii and S.B. Cronin, *Sensing Local pH and Ion Concentration at Graphene Electrode Surfaces using In Situ Raman Spectroscopy.* Nanoscale, DOI: 10.1039/C7NR08294K (2018).
32. Hou, B.Y., F. Rezaeifar, J. Qiu, G.T. Zeng, R. Kapadia and S.B. Cronin, *Prevention of surface recombination by electrochemical tuning of TiO2-passivated photocatalysts.* Applied Physics Letters, **111** (2017).
33. Hou, B.Y., L. Shen, H.T. Shi, R. Kapadia and S.B. Cronin, *Hot electron-driven photocatalytic water splitting.* Physical Chemistry Chemical Physics, **19**, 2877-2881 (2017).